PSFC/JA-03-15

Excitation and Emission of Electron Cyclotron Waves in Spherical Tori

A. K. Ram and A. Bers

August 2003

Plasma Science and Fusion Center
Massachusetts Institute of Technology
Cambridge, MA 02139 U.S.A.

This work was supported by the U.S. Department of Energy, Grant No. DE-FG02-91ER-54109, and by the U.S. Department of Energy jointly with the National Spherical Torus Experiment, Grant No. DE-FG02-99ER-54521.

Submitted for publication to *Nuclear Fusion*.

Excitation and Emission of Electron Cyclotron Waves in Spherical Tori

A. K. Ram and A. Bers

Plasma Science & Fusion Center, M.I.T., Cambridge, MA, 02139, U.S.A.

E-mail contact of main author: abhay@mit.edu

Abstract. The conventional ordinary and extraordinary modes in the electron cyclotron range of frequencies are not suitable for heating of and/or driving currents in spherical tori (ST) plasmas. However, electron Bernstein waves offer an attractive possibility for heating and current drive in this range of frequencies. In this paper, we summarize our theoretical and numerical results which describe the excitation of electron Bernstein waves in ST plasmas when the extraordinary mode or the ordinary mode are coupled into the plasma from an external source. In our discussion on the conversion of the ordinary mode to electron Bernstein waves (via the slow extraordinary mode) we illustrate very important physics, relevant to this conversion process, that has been ignored in previous studies. The particular physics has to do with the conversion of the slow extraordinary mode to the fast extraordinary mode that can then propagate out of the plasma and thus reduce the mode conversion to electron Bernstein waves. This reduction in the mode conversion can occur even when the wave numbers are such that the ordinary mode cutoff and the slow extraordinary mode cutoff are coincident in space. Furthermore, we also consider the emission of electron Bernstein waves from a thermal plasma. This emission mode converts to extraordinary and ordinary modes in the vicinity of the upper hybrid resonance. We describe the general relationship between the conversion coefficients when exciting electron Bernstein waves using either the extraordinary mode or the ordinary mode, and the emission coefficients when thermally emitted electron Bernstein waves convert to the extraordinary and ordinary modes.

1. Introduction

Plasmas in high-β spherical tori, e.g., in NSTX [1] and MAST [2], present a special experimental challenge when considering heating and current drive by waves in the electron cyclotron range of frequencies. This is primarily due to such plasmas being overdense, i.e., $\omega_{pe}/\omega_{ce} \gg 1$ where ω_{pe} and ω_{ce} are the electron plasma and electron cyclotron frequencies, respectively. For fundamental or second harmonic heating in such plasmas, the conventional extraordinary X mode and the ordinary O mode are cutoff near the edge of the plasma and cannot access the core. For higher harmonics the plasma is essentially transparent to the X and O modes.

Mode conversion near the plasma edge allows X or O mode polarized power, incident from free space, to couple to electron Bernstein waves (EBW). The X mode couples to EBWs in the vicinity of the upper hybrid resonance (UHR). The O mode coupling to EBWs is via the slow X mode whereby power from the externally excited O mode is first mode converted to the slow X mode which subsequently mode converts to EBWs near the UHR. The propagation of EBWs is not density limited and the waves damp effectively on electrons in the vicinity of the Doppler shifted electron cyclotron resonance (or its harmonics) [3]. In this paper, we discuss theoretical details of the constraints imposed on the mode conversion of X and O modes to the EBWs in spherical tori. We shall refer to the two conversion process as X-B and O-B, respectively, with an understanding that the O-B process requires an intermediate step whereby the O mode converts to the slow X mode.

From ray tracing, we have previously shown [3] that EBWs damp very effectively on electrons in the vicinity of the location of the Doppler-shifted electron cyclotron resonance (or its harmonics). Consequently, EBWs can also be emitted by a thermal plasma from near these absorption regions. Such EBWs can propagate out to the upper hybrid resonance at the edge of the plasma where they mode convert to the X and

O modes. The X and O modes propagate towards the lower density region, and the vacuum, at the edge where they become free space propagating modes and are observed in the region outside the plasma. A number of experiments have studied this emission of EBWs in spherical tori [4, 5, 6, 7, 8]. We have also shown that the mode conversion coefficients for EBW emission are directly related to the mode conversion coefficients for the excitation of EBWs by sources external to the plasma [9, 10]. This will be illustrated through results obtained from numerical solutions of a full-wave kinteic description of mode conversion among EBW and the X and O modes.

It is important to note that when we mention X and O modes in this paper we are really discussing "quasi X" and "quasi O" modes. It is only for purely perpendicular propagation across the ambient magnetic field that we have X and O modes – the X mode being elliptically polarized and the O mode being linearly polarized. For oblique propagation the polarizations are mixed. However, the two modes can still be clearly distinguished for oblique propagation.

2. Excitation of Electron Bernstein Waves — Cold Plasma Model

We can obtain important analytical results by first considering a simplified model in which the plasma is assumed to be cold and the poloidal magnetic field is ignored. The wave fields are assumed to be independent of any poloidal variations. Then the excitation of EBWs is studied in a slab geometry model where the x coordinate is in the direction of the inhomogeneity, y is along the poloidal direction, and z along the toroidal direction. Assuming that the magnetic field is along z, the propagation of waves in an inhomogeneous cold and collisionless plasma is given by

$$K_\perp \frac{d^2 E_y}{dx^2} + \frac{\omega^2}{c^2}\left(K_\perp^2 - K_X^2 - \frac{c^2}{\omega^2} k_\parallel^2 K_\perp\right) E_y = k_\parallel K_X F \quad (1)$$

$$\frac{d}{dx}\left[\frac{1}{K_\parallel}\frac{dF}{dx}\right] + \frac{\omega^2}{c^2}\left(1 - \frac{c^2}{\omega^2}\frac{k_\parallel^2}{K_\perp}\right) F = \frac{\omega^2}{c^2}\frac{K_X}{K_\perp} k_\parallel E_y \quad (2)$$

where $F = ik_\parallel E_x - dE_z/dx$, $dF/dx = (\omega^2/c^2)\, K_\parallel E_z$, c is the speed of light, ω is the wave frequency, $k_\parallel$ is the component of the wave vector $\vec{k}$ along the magnetic field $\vec{B} = \hat{z}B_0(x)$,

$$K_\perp = 1 - \frac{\omega_{pe}^2(x)}{\omega^2(x) - \omega_{ce}^2(x)}, \quad K_X = -\frac{\omega_{ce}(x)}{\omega}\left(\frac{\omega_{pe}^2(x)}{\omega^2 - \omega_{ce}^2(x)}\right), \quad K_\parallel = 1 - \frac{\omega_{pe}^2(x)}{\omega^2} \tag{3}$$

$\omega_{pe}(x)$ and $\omega_{ce}(x)$ are the electron plasma and cyclotron angular frequencies, respectively. The variation of the fields in the z directions is assumed to be of the form $\exp(ik_\parallel z)$ and the time dependence is assumed to be of the form $\exp(-i\omega t)$.

For the case when $k_\parallel = 0$, (1) and (2) are uncoupled and describe the propagation of the X mode and the O mode, respectively, across the magnetic field. The X mode equation (1) has a resonance at $K_\perp = 0$ corresponding to the UHR. Equation (1) also has two cutoffs corresponding to the zeros of $K_\perp^2 - K_X^2$. The resonance absorption of X mode power at the UHR corresponds to the power mode converted to the EBWs [3]. Since the O mode is completely decoupled from the X mode, if an O mode is excited at the edge there will be no resonance absorption. The power will be reflected back out at the O mode cutoff located at the position where $K_\parallel = 0$. In this analysis we also assume that there is no electron cyclotron resonance between the edge of the plasma and the cutoffs of the X and O modes. This is generally true in NSTX and MAST. Thus, the only absorption is at the UHR.

If we assume that, for sufficiently small $n_\parallel = ck_\parallel/\omega$, only the X mode is excited at the plasma boundary, then the equation for X mode propagation is approximately given by

$$\left(K_\perp - n_\parallel^2\right)\frac{d^2E_y}{dx^2} + \frac{\omega^2}{c^2}\left[\left(K_\perp - n_\parallel^2\right)^2 - K_X^2\right]E_y = 0\ . \tag{4}$$

This equation is obtained from (1) and (2) by assuming that $E_z \approx 0$. In this approximation the X mode resonance is no longer at $K_\perp = 0$ but at $K_\perp - n_\parallel^2 = 0$ which, for small $n_\parallel$, is a small correction. In this case (4) describes the propagation of the

X mode into a region of increasing density as it passes through the right-hand cutoff, the upper hybrid resonance, and the left-hand cutoff. We refer to this as the triplet cutoff-resonance-cutoff mode conversion process which has been discussed extensively in [11]. Following the recipe provided in [11], we find that the fraction of the power on the X mode that is converted to EBWs is given by

$$C_{XB}\left(\eta,\phi\right)=4e^{-\pi\eta}\left(1-e^{-\pi\eta}\right)\cos^{2}\left(\phi\right) \tag{5}$$

where

$$\phi=\frac{\pi}{2}+\frac{1}{2}\cos^{-1}\left(\frac{N_{R}^{2}-N_{I}^{2}}{N_{R}^{2}+N_{I}^{2}}\right) \tag{6}$$

$N\equiv N_R+iN_I$, with

$$\begin{aligned} N &= \ln\left(\frac{i\eta}{\eta_1}\right)+\pi\left[i\coth\left(\frac{\pi}{2}\eta\right)+\cot\left(\frac{\pi}{2}\eta_1\right)\right]-\frac{1}{\eta_1}-\frac{i}{\eta} \\ &\quad +\psi\left(1+\frac{\eta_1}{2}\right)-\psi\left(1+\frac{i\eta}{2}\right) \end{aligned} \tag{7}$$

ψ is the Psi function, and

$$\eta = \left(1-n_{\parallel}^{2}\right)^{3/2}\left[\frac{\omega_{ce}L_n}{c\alpha}\left(\sqrt{1+\alpha^2}-1\right)^{2}\right]_{UHR} \tag{8}$$

$$\eta_1 = \left(1-n_{\parallel}^{2}\right)^{3/2}\left[\frac{\omega_{ce}L_n}{c\alpha}\left(\sqrt{1+\alpha^2}+1\right)^{2}\right]_{UHR}. \tag{9}$$

In (8) and (9) the right-hand sides are evaluated at the UHR ($K_\perp=0$), L_n is the density scalelength, and $\alpha=\omega_{pe}/\omega_{ce}$.

In Figure 1 we plot

$$C_{XB}^{(max)}=4e^{-\pi\eta}\left(1-e^{-\pi\eta}\right) \tag{10}$$

as a function of η. This gives the envelope of (5), i.e., the maximum possible fractional power of the X mode that can be mode converted to EBWs. Alternatively, from (5), $C_{XB}^{(max)}=C_{XB}\left(\eta,n\pi\right)$ where n is any integer including zero. For $\eta\approx 0.22$, $C_{XB}^{(max)}=1$ which implies that all of the X mode power is converted to EBW. From Fig. 1 we note

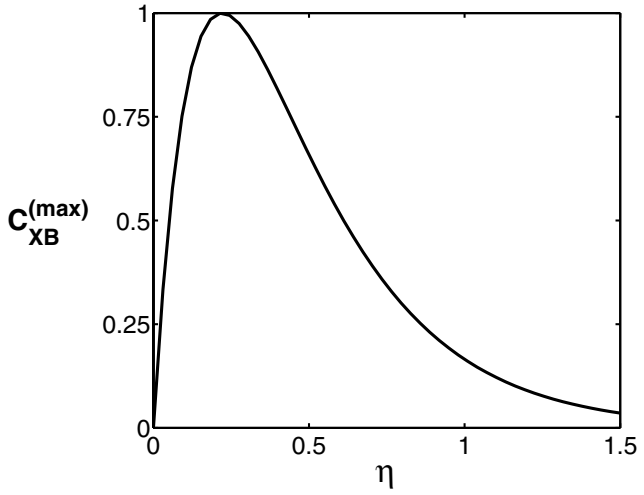

Figure 1: $C_{XB}^{(max)}$ as a function of η

that $C_{XB}^{(max)} \geq 0.5$ if $0.05 \lesssim \eta \lesssim 0.6$. For $n_{\|} = 0$, from (8) we find that the necessary condition for the X-B mode conversion to be better than 50% requires

$$0.013 \text{ T cm} \lesssim |BL_n|_{UHR} \lesssim 0.16 \text{ T cm} \tag{11}$$

This shows that the X-B mode conversion process is efficient for sharp density gradients, i.e., short density scalelengths. As $n_{\|}$ is increased from zero, the fraction of the X mode power that is coupled to EBWs decreases.

From (2), it is clear that for $k_{\|} = 0$ the O mode does not couple power to the EBW. For the O mode power to couple to EBW, it is necessary to have oblique propagation of the O mode, i.e., $k_{\|} \neq 0$. Then the O mode power can couple to the X mode which, in turn, can undergo resonance absorption. The necessary condition for optimum coupling of the O mode power to the X mode is [12]

$$n_{\|,c} = \frac{ck_{\|}}{\omega} = \left[\left(1 + \frac{\omega}{\omega_{ce}}\right)^{-1/2}\right]_c \tag{12}$$

where the right-hand side is to be evaluated at the spatial location where $\omega = \omega_{pe}$. However, in order for the O mode power not to get reflected back out on the X mode

requires that $\eta > 1$ [3, 9]. From (8) we find that this condition is satisfied when the density scalelength is longer than that required for optimum mode conversion from the X mode.

From the above discussion, we conclude that the X-B and the O-X-B mode conversion processes are optimized in different regions of the two-dimensional parameter space spanned by wave frequency and parallel wavelength, and at different locations inside the plasma. The X-B mode conversion process is optimized for $k_{\|} \approx 0$ and wave frequencies which place the UHR in the short density scalelength region. The O-X-B mode conversion process is optimized for $k_{\|}$ given in (12) and for wave frequencies which place the UHR in a longer density scalelength region of the plasma. The optimum X-B process occurs closer to the edge of the plasma than the optimum O-X-B conversion.

3. Excitation of Electron Bernstein Waves — Kinetic Plasma Model

We extend the analysis of the previous section to include the EBW explicitly into the mode conversion equations. Furthermore, we will explicitly include the poloidal magnetic field as this forms an important component of the mode conversion equations in a ST plasma. The development of the approximate kinetic analysis has been detailed previously [3, 9, 13]. Here we just provide the basic equations for completeness.

The equilibrium magnetic field is assumed to be sheared with the form

$$\vec{B}_0(x) \equiv B_y(x)\hat{y} + B_z(x)\hat{z} = B_0(x)\sin\Psi(x)\hat{y} + B_0(x)\cos\Psi(x)\hat{z} \tag{13}$$

where Ψ is the angle between $\vec{B}_0$ and the z-axis. The variation of the fields in the y and z directions is assumed to be of the form $\exp(ik_y y + ik_z z)$ where k_y and k_z are the appropriate components of the wave vectors. The approximate full wave description of the propagation of the X mode, O mode, and the EBWs is given by

$$\frac{d\vec{F}}{d\xi} = i \overleftrightarrow{A}_K \cdot \vec{F} \tag{14}$$

where $\xi = \omega x/c$ is the normalized spatial variable,

$$\vec{F}^{\,T} = [E_x \; E_y \; E_z \; (i\chi_1 E_x') \; cB_z \; (-cB_y)] \tag{15}$$

is the transpose of the field vector $\vec{F}$, $E_x' = (dE_x/d\xi)$,

$$\overleftrightarrow{A}_K = \begin{bmatrix} 0 & 0 & 0 & -\chi_1^{-1} & 0 & 0 \\ n_y & 0 & 0 & 0 & 1 & 0 \\ n_z & 0 & 0 & 0 & 0 & 1 \\ K_{xx} & \chi_{xy} & \chi_{xz} & 0 & n_y & n_z \\ -\chi_{xy} & K_{yy} - n_z^2 & \chi_{yz} + n_y n_z & 0 & 0 & 0 \\ -\chi_{xz} & \chi_{yz} + n_y n_z & K_{zz} - n_y^2 & 0 & 0 & 0 \end{bmatrix} \tag{16}$$

$$\overleftrightarrow{K} = \overleftrightarrow{I} + \overleftrightarrow{\chi} \tag{17}$$

$$\overleftrightarrow{\chi} = \frac{-\omega_p^2}{(\omega^2 - \omega_c^2)} \begin{pmatrix} 1 & -i\omega_{cz}/\omega & i\omega_{cy}/\omega \\ i\omega_{cz}/\omega & 1 - \omega_{cy}^2/\omega^2 & -\omega_{cy}\omega_{cz}/\omega^2 \\ -i\omega_{cy}/\omega & -\omega_{cy}\omega_{cz}/\omega^2 & 1 - \omega_{cz}^2/\omega^2 \end{pmatrix} \tag{18}$$

where $\omega_p(x)$ is the electron plasma angular frequency, $\omega_{cy}(x) = eB_y(x)/m_e$ $\omega_{cz}(x) = eB_z(x)/m_e$ are the electron cyclotron angular frequencies for the poloidal and toroidal fields, respectively, $\omega_c = \sqrt{\omega_{cy}^2 + \omega_{cz}^2}$, $n_y = ck_y/\omega$, $n_z = ck_z/\omega$,

$$\chi_1 = \left(\frac{v_T}{c}\,\frac{\omega_p}{\omega_c}\right)^2 \left(\frac{\omega^2}{\omega^2 - \omega_c^2} - \frac{\omega^2}{\omega^2 - 4\omega_c^2}\right) \tag{19}$$

and $v_T = \sqrt{T(x)/m_e}$ is the electron thermal velocity corresponding to the temperature $T(x)$.

The only component of the electromagnetic wave field whose evolution is not given by (14) is B_x, which can be obtained from Faraday's equation [9]

$$cB_x = n_y E_z - n_z E_y \tag{20}$$

Thus, the kinetic full-wave dynamics given by (14)–(20) describe the coupling between the X mode, the O mode, and the EBW, i.e., the kinetic mode conversion process. The procedure to solve these equations numerically with the appropriate boundary conditions has been detailed in [9].

The total, electromagnetic and kinetic, time-averaged energy flow density in the x-direction is [3, 13]

$$\langle \vec{s} \rangle_x = \frac{1}{4}\sqrt{\frac{\epsilon_0}{\mu_0}}\ \vec{F}^{\,\dagger} \cdot \overleftrightarrow{R} \cdot \vec{F} \tag{21}$$

where $\vec{F}^{\,\dagger}$ is the transpose of the complex conjugate of $\vec{F}$ and

$$\overleftrightarrow{R} = \left[\begin{array}{ccc|ccc} & & & 1 & 0 & 0 \\ & 0 & & 0 & 1 & 0 \\ & & & 0 & 0 & 1 \\ \hline - & - & - & - & - & - \\ 1 & 0 & 0 & & & \\ 0 & 1 & 0 & & 0 & \\ 0 & 0 & 1 & & & \end{array}\right] . \tag{22}$$

Then, from (14) we find that

$$\frac{d}{d\xi}(\vec{F}^{\,\dagger} \cdot \overleftrightarrow{R} \cdot \vec{F}) = 0 \tag{23}$$

This equation is needed to ensure that the numerical scheme solving the mode conversion equations is conserving the total, electromagnetic and kinetic, time-averaged energy flow density. The conservation condition is consistent with the assumption that there is no damping in the mode conversion region; i.e., we assume that the EBW damping at the Doppler shifted electron cyclotron harmonic occurs away from the mode conversion region inside the plasma.

In the plasma region away from where the mode conversion occurs, the solutions to (14) can be obtained using the WKB technique. In this case the X mode, the O mode,

and the EBW are distinctly identifiable, and the energy flow density along these waves can be determined using (21). The various mode conversion coefficients are obtained by the appropriate ratios of these energy flow densities.

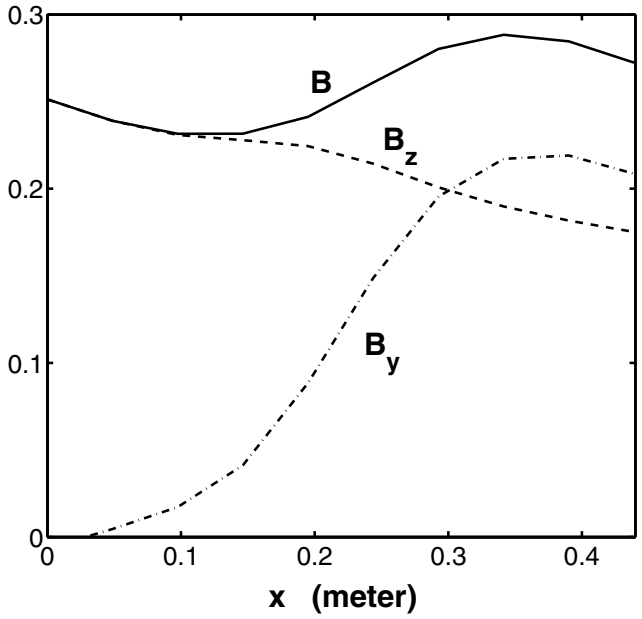

Figure 2: The magnitudes of the poloidal component B_y (dot-dashed), the toroidal component B_z (dashed), and the total magnetic field B (solid line) in Tesla as a function of the minor radius. $x = 0$ is the center of the plasma and $x = 0.44$ m is the outside edge of the plasma.

The mode conversion equations (14)–(20) are not amenable to analytical solutions. We have to resort to a fully numerical integration of (14)–(20) with the appropriate boundary conditions. To illustrate the physics involved in the mode conversion coupling between the X mode, the O mode, and the EBWs, we will study numerical solutions obtained for NSTX-type parameters [3] corresponding to a high-β scenario. The specific plasma parameters are as follows. The Shafranov-shifted major radius is $R = 1.05$ m, the minor radius is $a = 0.44$ m, the peak electron density is $n_0 = 3 \times 10^{19}$ m^{-3}, the

peak electron temperature is $T_0 = 3$ keV, the density profile is $n_e = n_E + (n_0 - n_E)(1 - x^2/a^2)^{1/2}$, and the temperature profile is $T_e = T_E + (T_0 - T_E)(1 - x^2/a^2)^2$, where n_E and T_E are the edge density and temperature, respectively, with $n_E/n_0 = 0.02$ and $T_0/T_E = 0.02$. The magnetic field profile is taken to be that shown in Figure 2

4. Mode Conversion to Electron Bernstein Waves — No poloidal field

Let us consider the coupling of an externally launched X mode or O mode to EBWs. To test our analytical analysis of the previous section we will assume that, in (13), $\Psi(x) \equiv 0$ and B_0 is the same as B shown in Figure 3. This primarily eliminates the effect of the poloidal field on the mode conversion process and simplifies the analysis. The influence of the poloidal field on mode conversion will be addressed in a subsequent section. In what follows in this section we will set $n_y = 0$ so that, consequently, $n_z = n_\parallel$ is the wave number along the magnetic field. Without the poloidal magnetic field the y-variation is not needed since one can transform to a frame where the z-axis is along the magnetic field and the x-axis is perpendicular to it.

4.1. Mode Conversion from an X mode

Figure 3 compares the power mode conversion coefficient to EBWs from the X mode for a range of frequencies. In this figure $C_{XB}^{(max)}$ as obtained from (10), C_{XB} as obtained from (5)–(9), and $C_{XB}^{(k)}$ as obtained from the numerical solution of (14)–(20). For frequencies below about 15.5 GHz, $C_{XB}^{(k)}$ is bounded by $C_{XB}^{(max)}$ and and C_{XB}. This indicates that the theoretical maximum C_{XB} is also a maximum of the kinetic mode conversion process. Also, the analytical calculation of the phase in (5) is reasonably good. For frequencies greater than about 16 GHz there are differences between the analytical estimates and the kinetic numerical results. The reason for this difference is simple. For frequencies below 15.5 GHz the UHR is between the first and second

harmonics of the electron cyclotron frequencies. For frequencies above 15.5 GHz the UHR is between the second and third harmonics of the electron cyclotron frequency. As the UHR frequency ω_U transits through these domains the character of the kinetic dispersion relation changes [9]. For $\omega_U < 2\omega_{ce}$ the slow X mode couples to the EBW at the UHR and does not propagate past the UHR towards the low density region of the plasma. For $\omega_U > 2\omega_{ce}$ the slow X mode propagates through the UHR towards the lower density region and couples to the backward propagating EBW closer to the edge of the plasma than the location of the UHR. This change in the character of the slow X mode coupling to the EBW is not part of the cold plasma description. It appears only in the kinetic formulation (see Figs. 6 and 7 in[9]). For $\omega_U < 2\omega_{ce}$ the mode conversion region is described by a cutoff-resonance-cutoff triplet, [9, 11] while for $\omega > 2\omega ce$ the propagation of the slow X mode through the UHR changes the description to a cutoff-cutoff doublet [9]. The oscillations in $C_{XB}^{(k)}$ are possibly due to the change in wave phase between the cutoffs. It is difficult to develop an analytical picture as the conversion equation, even for perpendicular propagation, is at least fourth order. Even though the wave properties change for $\omega_U > 2\omega_{ce}$, $C_{XB}^{(max)}$ still represents, approximately, the maximum power mode conversion coefficient. In plotting $C_{XB}^{(k)}$ in Fig. 3 there is a gap around 15.5 GHz. Around this frequency the second electron cyclotron harmonic transits through the mode conversion region. Since electron cyclotron damping is not included in the formulation of the kinetic mode conversion equations [9], we do not carry out any computations in this region. An important reason for not including damping in the kinetic formulation is that it would not be desirable to have electron cyclotron resonances near the mode conversion region in actual experiments. The presence of such resonances would inhibit the mode conversion process and lead to electron absorption near the edge of the plasma where mode conversion in STs will take place.

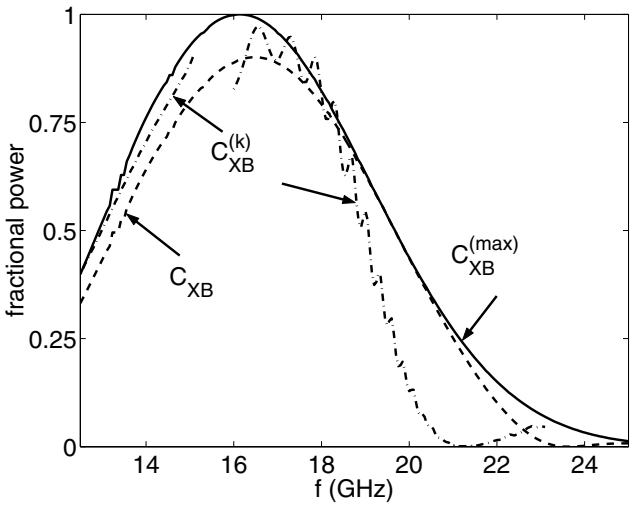

Figure 3: A comparison of $C_{XB}^{(max)}$ (solid line) and C_{XB} (dashed line), from (5)–(9), as a function of the X mode frequency for NSTX-type parameters. $C_{XB}^{(k)}$ (dot-dashed line) is the power mode conversion coefficient obtained from the numerical solution of the kinetic equations (14)–(20).

Let us consider the mode conversion at a particular frequency and as a function of the toroidal wave number n_z. In Fig. 4 we plot the various power conversion coefficients for an incoming X mode frequency of 16.5 GHz. For $n_z = 0$ there is no coupling to the O mode as the power reflection coefficient R_{XO} is zero. This is consistent with Eqs. (1) and (2) where, for $n_\parallel \equiv n_z = 0$ the O mode equation (2) is completely decoupled from the X mode equation (1). For small n_z there is essentially no power coupled to the O mode.

From Fig. 3 we note that the conversion of the X mode to EBWs is most effective for frequencies around 16 GHz. This corresponds to the conversion layer being nearer the edge of the plasma where the density gradients are steep and the density scalelength is close to the critial value where, from Eq. (8) $\eta \approx 0.22$. For higher frequencies, the

mode conversion region moves farther into the plasma where the density scalelength at the UHR are becoming long and $\eta \gg 0.22$. For lower frequencies the mode conversion region moves farther out towards the edge of the plasma where the density scalelength at the UHR is becoming short and $\eta < 0.22$.

From Fig. 4 we observe that, for a given frequency, the mode conversion of the X mode to EBWs is effective for a broad range of n_z with the maximum occurring for purely perpendicular propagation when there is no coupling to the O mode.

From Figs. 3 and 4 we conclude that the conversion of the X mode to EBWs is most effective when the conversion region is nearer the edge of the plasma

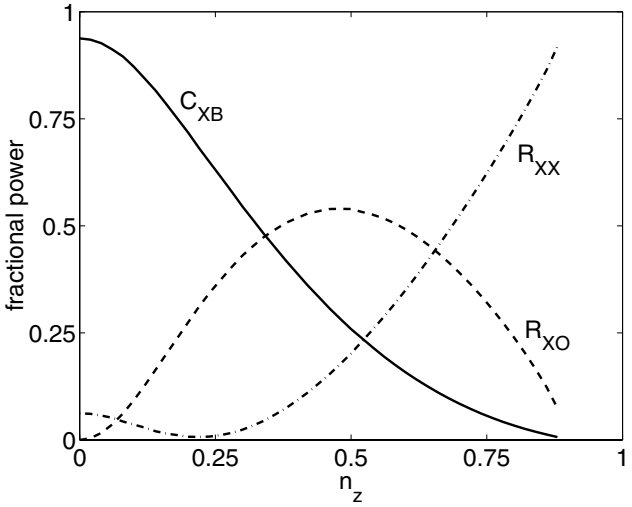

Figure 4: Power conversion coefficients as a function of n_z, for an externally launched X mode, as obtained from the numerical solution of the kinteic equations. C_{XB} is the fractional power mode converted to EBWs, and R_{XX} and R_{XO} are the fractional powers reflected out on the X mode and O mode, respectively. The X mode frequency is 16.5 GHz.

4.2. Mode Conversion from an O mode

The conversion of O mode to the slow X mode has been extensively studied, theoretically, in the literature [12, 15, 16, 17, 18, 19]. The coupling of O mode power to slow X mode occurs near a critical parallel wave number, given by Eq. (12), when the left-hand X cutoff is near the O mode cutoff [12]. The previous studies have primarily looked at the transmission coefficient from the O mode to the slow X mode through the two respective cutoffs [12, 15, 16, 18, 19]. It is then assumed that the O mode power that tunnels to the slow X mode will couple to the EBW at the UHR. The transmission coefficient is dependent on the density scalelength in the vicinity of the cutoffs and the range of parallel wavenumbers that can lead to effective transmission of the O mode to the slow X mode increases as the density scalelength decreases [16, 19]. These studies completely ignore the possibility that the slow X mode, in the vicinity of the UHR, can couple power to the fast X mode which, subsequently, propagates out to the edge of the plasma and reduces the power available to the EBWs. For small scalelengths the right-hand X mode cutoff moves closer to the UHR reducing η in Eq. (8). This increases the tunneling of the slow X mode to the fast X mode. So the condition for coupling effectively from the O mode to the slow X mode requires that the fast X mode cutoff be sufficiently removed from the UHR, i.e., $\eta > 1$, or long scalelengths.

Figure 5 shows the power conversion coefficients, as a function of n_z when an O mode, with a frequency of 16.5 GHz, is launched into the plasma. From Eq. (12), the critical value of $n_{z,c} \equiv n_{\parallel,c}$ is approximately 0.57. In the proximity of this critical value we note that the reflection on the O mode R_{OO} is nearly zero and the mode converted power C_{OB} is a maximum. However, this maximum value is less than 0.5 which implies that less than half of the input O mode power is being coupled to the EBWs even though we are at the optimum $n_{\parallel}$. The rest of the power is being reflected back out on the X mode and is indicated by R_{OX}. This important effect has been completely ignored in

previous studies of O-B mode conversion and is very important to properly understand the mode conversion of the O mode to EBWs via the slow X mode.

If we increase the O mode frequency to 28 GHz, the corresponding power coversion coefficients are plotted in Fig. 6. For this frequency the critical value of $n_{z,c} \equiv n_{\|,c}$ is approximately 0.47. We now note, from C_{OB}, that nearly all of the O mode power is converted to the EBWs. The reflection out on the X mode R_{OX} is small. When C_{OB} is a maximum R_{OO} is a minimum. From numerical calculations we find that 28 GHz is approximately the lowest frequency where 100% mode conversion is possible in the O-B mode conversion scenario. This corresponds to higher harmonic resonances being inside the plasma than for the case of optimized X-B conversion.

A comparison of Figs. 5 and 6 provides a physical insight into the conversion of the O mode to EBWs. The range of n_z's for which C_{OB} is about 50% of its maximum value increases as the frequency decreases. A decrease in the frequency moves the mode conversion region farther towards the edge of the plasma into the region of small density scalelengths. This picture is consistent with previous theories on the conversion of O mode to EBWs [12, 15, 16, 18, 19]. However, the maximum power mode conversion coefficient decreases with decreasing frequency as power reflected on the X mode, R_{OX}, increases. The reflection coefficient R_{OX} is proportional to $\exp(-\pi\eta)$ with η given in Eq. (8). As the scalelength becomes smaller, η becomes smaller and R_{OX} increases. Thus, for efficient conversion of O mode power to EBWs, it is not only necessary to have a critical $n_{\|,c}$, given by (12), but, importantly, to also have $\eta > 1$.

A comparison of the X-B and O-B conversion processes shows that the X-B conversion is optimized for lower frequencies leading to the mode conversion region being in the short density scalelength part of the plasma. The optimum O-B conversion requires longer density scalelengths and ocurrs farther into the plasma. Furthermore, the X-B

mode conversion process is efficient over a wider range of parallel wavenumbers than the O-B conversion process.

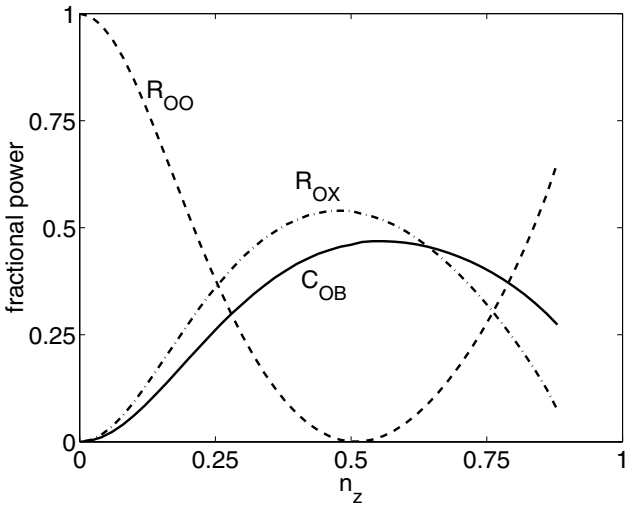

Figure 5: Power conversion coefficients as a function of n_z, for an externally launched O mode, as obtained from the numerical solution of the kinteic equations. C_{OB} is the fractional power mode converted to EBWs, and R_{OX} and R_{OO} are the fractional powers reflected out on the X mode and O mode, respectively. The O mode frequency is 16.5 GHz.

5. Mode Conversion to Electron Bernstein Waves — Effects of poloidal field

Let us now study the changes in the mode conversion process due to the poloidal magnetic field. This also requires that we include the effect of the poloidal wave numbers n_y. The parameters used for our studies are NSTX-type discussed earlier and the magnetic field is as shown in Fig. 2. The major effect of including the poloidal field is that the power flow mode conversion coefficients are no longer symmetric in n_z (or n_y). In Fig. 7 we plot the fractional power mode converted to EBWs from an X mode, C_{XB}, as function of n_y for three different values of n_z. The asymmetry in both n_y and

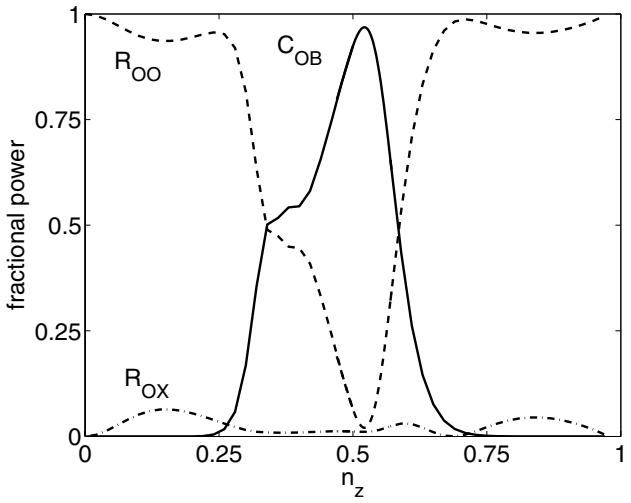

Figure 6: Same as Fig. 5 except that the the O mode frequency is 28.0 GHz.

n_z is evident. This asymmetry is further amplified for the O-B conversion process as illustrated in Fig. 8. (In the case of Fig. 6, corresponding to no poloidal field, the conversion coefficients are found to be completely symmetric around $n_z = 0$.) For the O-B conversion process it is important to choose the O mode launch angle appropriately with respect to the poloidal field and the toroidal field. For X-B conversion there is a broad range of n_y and n_z for effective conversion to EBWs.

6. Emission of Electron Bernstein Waves

From ray tracing analysis we have shown that EBWs are locally and strongly absorbed at the Doppler shifted electron cyclotron resonance or its harmonics [3]. The strong and localized absorption implies that thermal emission of EBWs can occur for frequencies corresponding to the local Doppler-shifted electron cyclotron frequency. This emission then converts, at the UHR, to the X and O modes which are then observed in the vacuum region. The excitation and emission of EBWs has been observed experimentally on spherical tori [4, 5, 6, 7, 8].

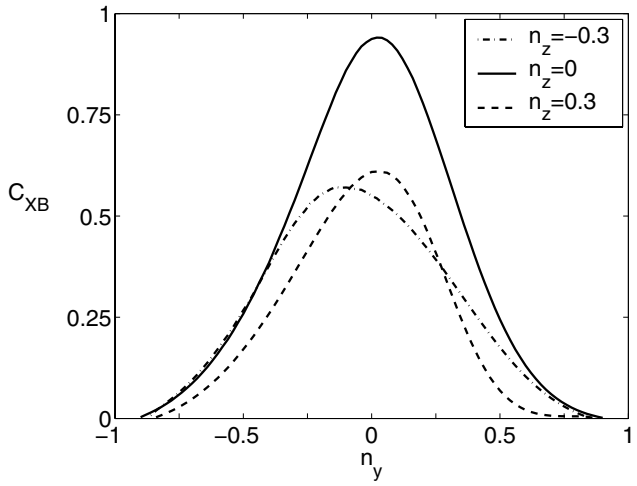

Figure 7: Fractional power mode converted to EBWs C_{XB} as a function of n_y, for an externally launched X mode for three different values of n_z. The wave frequency is 16.5 GHz and the poloidal field is included in the calculations.

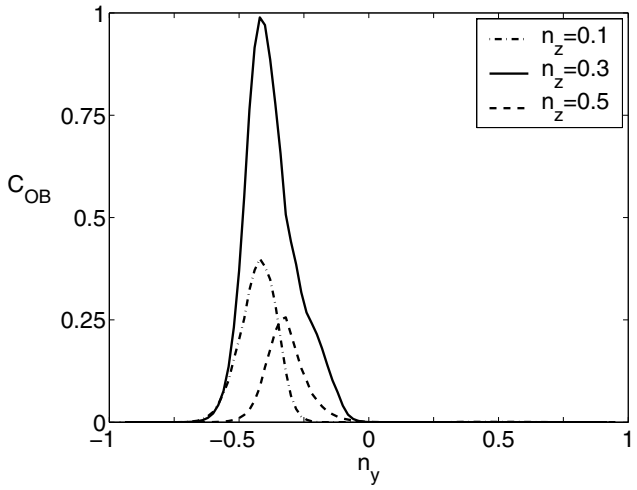

Figure 8: Fractional power mode converted to EBWs C_{OB} as a function of n_y, for an externally launched O mode for three different values of n_z. The wave frequency is 28 GHz and the poloidal field is included in the calculations.

The kinetic model we have developed allows us to study the mode conversion of emitted EBWs to X and O modes. This is not possible in the cold plasma model where the power flow conversion coefficient to the EBW is given by the power resonantly absorbed at the UHR. In order to study the emission we need to have a proper description of the EBWs.

Figure 9 shows the mode conversion emission coefficients for an EBW propagating out to the edge and converting to X and O modes at the UHR. The emission coefficients of the X and O modes are given by E_X and E_O, respectively, and R_B is the fraction of the emitted EBW that is reflected back into the plasma. The results in Fig. 9 are for the case of no poloidal field and the parameters are similar to those in section 4 above.

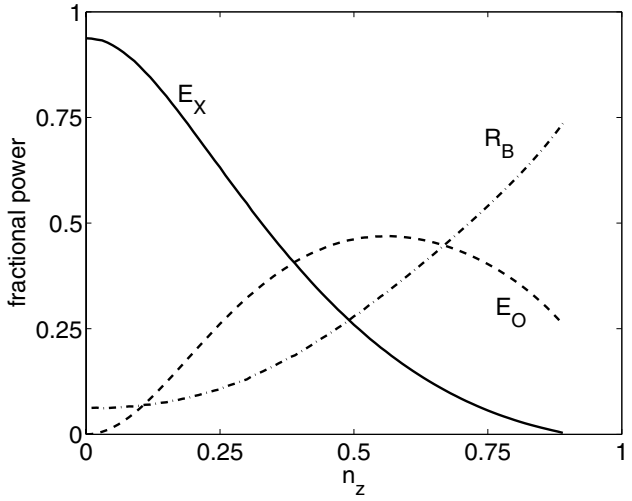

Figure 9: Power mode conversion emission coefficients as a function of n_z for the case of no poloidal field. The emitted EBW wave frequency is assumed to be 16.5 GHz. E_X and E_O are fractions of the emitted EBW power that is converted to the X and O modes, respectively. R_B is the fraction of EBW emitted power that is reflected back into the plasma.

If we compare Fig. 9 with Figs. 4 and 5 it becomes evident that

$$E_X = C_{XB} \quad \text{and} \quad E_O = C_{OB} \tag{24}$$

In other words, the fraction of the the X mode power flow that is mode converted to EBWs when an X mode is launched from the low density side is the same as the emitted EBW energy flow that is mode converted to an X mode that propagates out into the low density region. Similarly, the fraction of the O mode energy flow that is mode converted to EBWs when an O mode is launched from the low density side is the same as the emitted EBW energy flow that is mode converted to an O mode that propagates out into the low density region. The emitted X and O modes propagate out into the vaccum region where they are observed in experiments.

Also upon comparing Figs. 4 and 5 we note that

$$R_{XO} = R_{OX} \tag{25}$$

This implies that for an X mode launched from the outside, the fraction of the X mode power that is reflected back out on the O mode is the same as the fraction of the O mode power that is reflected back out on the X mode for an O mode launched from the outside,

The symmetry relations in (24) and (25) are, in fact, quite general and can be derived, from first principles, using considerations of energy flow conservation and energy flow under time reversal [9, 10]. Thus, the symmetry relations hold even for the case when the effect of the poloidal field is included in our studies of mode conversion.

The equality between the emission coefficients and the excitation coefficients also points to the fact that optimized mode conversion heating and current drive experiments can be designed on the basis of the optimized emission results. The conditions for which the X mode (or the O mode) emission is most pronounced will be the conditions for

which the X-B (or the O-B) mode conversion is maximized.

7. Conclusions

From our studies of the mode conversion process in which power from an externally launched X mode or O mode can be coupled to EBWs in a ST plasma, we note that the two processes, X-B and O-B, are optimized in different regions of parameter space spanned by the parallel wave numbers and the wave frequency. The X-B conversion is optimized for a broad range of parallel wave numbers with a peak at, or near, perpendicular (to the magnetic field) propagation. The O-B conversion process is optimized over a narrower range of parallel wave numbers and peaks around a criticial parallel wave number for which the O mode cutoff and the left-hand X mode cutoff coincide. Furthermore, the O-B conversion process is a maximum at a higher wave frequency compared to the X-B conversion process. Consequently, the O-B conversion takes place farther into the plasma than the X-B conversion. This implies that the density gradient scalelength within the mode conversion region is longer for the O-B process than for the X-B process. If the O-B process is moved into the region of short density scalelengths, part of the O mode power is reflected back out on the X mode. This effect has been ignored in previous studies. These studies showed that the short density scalelengths in the mode conversion region increased the range of parallel wave numbers for which the O-B conversion process was efficient. They completely ignored the coupling of the slow X mode to the fast X mode which neutralizes this proposed advantage.

We have shown that the mode conversion emission coefficients are related to the mode conversion excitation coefficients. This symmetry is very useful from an experimental point of view. Optimized mode conversion heating and current drive experiments can be designed on the basis of the emission results. The conditions for which the X mode (or the O mode) emission is most pronounced will be the conditions for which the X-B

(or the O-B) mode conversion is maximized.

8. Acknowledgments

This work is supported by U.S. Department of Energy Contracts DE-FG02-91ER-54109 and DE-FG02-99ER-54521.

References

[1] Ono, M., Kaye, S., Peng, M., *et al.*, in *Proceedings of the 17th International Atomic Energy Agency Fusion Energy Conference,* (International Atomic Energy Agency, Vienna, 1999), Vol. 3, p. 1135.

[2] Sykes A., in *Proceedings of the 17th International Atomic Energy Agency Fusion Energy Conference,* (International Atomic Energy Agency, Vienna, 1999), Vol. 1, p. 129.

[3] Ram, A. K., Schultz, S. D., Phys. Plasmas **7** (2000) 4084.

[4] Taylor, G., Efthimion, P. C., Jones, B., *et al.*, Phys. Plasmas **9** (2002) 167.

[5] Chattopadhyay, P. K., Andersen, J. K., Biewer, T. M., *et al.*, Phys. Plasmas **9** (2002) 752.

[6] Shevchenko, V., Cunningham, G., Field, A., in *Abstracts of Invited and Contributed Papers, 28th European Physical Society (EPS) Conference on Controlled Fusion and Plasma Physics,* edited by C. Silva, C. Varandas, and D. Campbell, (European Physical Society, 2001) pg. 381; ⟨http://www.cfn.ist.utl.pt/EPS2001/fin/pdf/p3.101.pdf⟩.

[7] Jones, B., Efthimion, P. C., Taylor, G., *et al.*, Phys. Rev. Lett. **90** (2003) 165001.

[8] Taylor, G., Efthimion, P. C., Jones, B., *et al.*, Phys. Plasmas **10** (2003) 1395.

[9] Ram, A. K., Bers, A., Lashmore-Davies, C. N., Phys. Plasmas **9** (2002) 409.

[10] Bers, A., Ram, A. K., Phys. Lett. A **301** (2002) 442.

[11] Ram, A. K., Bers, A., Schultz, S. D., Fuchs, V., Phys. Plasmas **3** (1996) 1976.

[12] Preinhaelter, J., and Kopecky, V., J. Plas. Phys. **10** (1973) 1.

[13] Bers, A., Ram, A. K., Schultz, S. D., RF Heating and Current Drive of Fusion Devices 1998 (Proc. 2nd Europhysics Topical Conf. Brussels, Belgium, 1998), (Jacquinot, J., et. al., Eds.), Vol. 22A, EPS, Petit-Lancy (1994) 237–240

[14] Ram, A. K., Bers, A., Phys. Fluids B **3** (1991) 1059.

[15] Weitzner, H., Batchelor, D. B., Phys. Fluids **22** (1979) 1355.

[16] Mjoljus, E., J. Plasma Physics **31** (1984) 7.

[17] Tokman, M. D. Sov. J. Plasma Physics **11** (1985) 689.

[18] Hansen, F. R., Lynov, J. P., Mardi, C., Petrillo, V., J. Plasma Phys. **39** (1988) 319.

[19] Cairns, R. A., Lashmore-Davies, C. N., Phys. Plasmas **7** (2000) 4126.